Atmos. Chem. Phys. Discuss., 10, 29113–29152, 2010
www.atmos-chem-phys-discuss.net/10/29113/2010/
doi:10.5194/acpd-10-29113-2010

Atmospheric Chemistry and Physics Discussions

Space-based evaluation of interactions between pollution plumes and low-level Arctic clouds during the spring and summer of 2008

K. Tietze[1,†], **J. Riedi**[2], **A. Stohl**[3], **and T. J. Garrett**[1]

[1]Univ. of Utah, Dept. of Atmospheric Sciences, Utah, USA
[2]Laboratoire d'Optique Atmosphérique, Université de Lille1/CNRS, France
[3]Norwegian Institute for Air Research, Kjeller, Norway
[†]deceased

Received: 2 November 2010 – Accepted: 16 November 2010 – Published: 26 November 2010

Correspondence to: T. J. Garrett (tim.garrett@utah.edu)

Published by Copernicus Publications on behalf of the European Geosciences Union.

Abstract

This study explores the indirect effects of anthropogenic and biomass burning aerosols on Arctic clouds by co-locating a combination of MODIS and POLDER cloud products with output from the FLEXPART tracer transport model. During the activities of the International Polar Year for the Spring and Summer of 2008, we find a high sensitivity of Arctic cloud radiative properties to both anthropogenic and biomass burning pollution plumes, particularly at air temperatures near freezing or potential temperatures near 286 K. However, the sensitivity is much lower at both colder and warmer temperatures, likely due increases in the wet scavenging of cloud condensation nuclei: the pollution plumes remain but the component that influences clouds has been removed along transport pathways. The analysis shows that, independent of temperature, cloud optical depth is approximately four times more sensitive to changes in pollution levels than is cloud effective radius. This suggests that some form of feedback mechanism amplifies the radiative response of Arctic clouds to pollution through changes in cloud liquid water path.

1 Introduction

In the Arctic, elevated concentrations of aerosol particles and trace gases occur seasonally every winter and spring due to a combination of long-range transport of anthropogenic and biomass burning emissions and slow aerosol pollutant removal rates (Quinn et al., 2007). A persistent wintertime surface temperature inversion inhibits vertical mixing and turbulent aerosol deposition, and the dryness of the Arctic atmosphere results in minimal wet scavenging (Law and Stohl, 2007). The Arctic haze rapidly dissipates in the spring, primarily due to the increased efficiency of wet scavenging in the warmer weather (Garrett et al., 2010), although reduced transport efficiency from mid-latitudes also plays a role.

ACPD
10, 29113–29152, 2010

Aerosols transported to the Arctic from lower latitudes can act as Cloud Condensation Nuclei (CCN). Enhanced CCN levels can increase cloud droplet number concentrations and decrease average droplet size relative to cleaner conditions (Hobbs et al., 2000). Over dark oceans, this can make clouds brighter and therefore have a cooling effect (Twomey, 1977). However, surface cooling is thought to be small in the Arctic due to low pollution levels during the summer and generally a highly reflective surface (Garrett et al., 2002). A more significant aerosol indirect effect probably involves changes in cloud thermal emission. Thin low level clouds have increased thermal emissivity under polluted conditions so that enhanced levels of CCN can possibly have a significant warming effect (Lubin and Vogelmann, 2006; Garrett and Zhao, 2006; Mauritsen et al., 2010).

Additionally, elevated aerosol concentrations have been thought to affect precipitation and cloud lifetime. Smaller droplet sizes suppress the collision-coalescence processes responsible for warm rain initiation, increasing the cloud water content and lengthening the lifetime of the cloud (Albrecht, 1989; Radke et al., 1989; Kaufman et al., 2005). However, further studies have shown that due to a myriad of dynamical considerations, there is no simple association between aerosol concentrations, precipitation and cloud liquid water content (Durkee et al., 2000; Ackerman et al., 2004; Lu and Seinfeld, 2005). For example, Xue and Feingold (2006) used model simulations to find that, although elevated aerosol concentrations tend to suppress precipitation, there is also an overall reduction in cloudiness due to stronger evaporation of the smaller cloud droplets and an increase in the entrainment of dry air.

For a comprehensive examination of aerosol-cloud interactions, space based measurements can be particularly useful since they provide sufficient statistics to tease a weak signal from a naturally noisy system. However, one downside of using passive spaceborne measurements alone to study aerosol-cloud interactions is that it is not possible to study clouds and aerosols that are vertically and horizontally coincident since clouds are so much brighter. For example, a commonly employed strategy is to pair cloud retrievals with aerosol retrievals from nearby adjacent airmasses. The

ACPD
10, 29113–29152, 2010

implicit assumption is that aerosol concentrations are horizontally homogeneous so that the two retrievals can be meaningfully compared (Sekiguchi et al., 2003; Quaas et al., 2004; Kaufman et al., 2005).

What is perhaps preferable is to examine the pollution field from a tracer transport model with cloud properties from co-located satellite measurements (e.g., Avey et al., 2007; Brioude et al., 2009). While this method relies on the accuracy of the transport model, the major advantage of this approach is that the clouds and pollution fields can be compared under the same meteorological conditions. Also, if the model pollution tracer is strictly passive within dynamic flows, it can be treated as an independent quantity that is unaffected by clouds, chemical processes and precipitation removal. Avey et al. (2007) used this method to study pollution-cloud interactions off the eastern seaboard of the United States. The comparison showed that the sensitivity of cloud effective radius and optical depth to anthropogenic pollution plumes decreases with increasing distance from emission sources. It was inferred that wet scavenging had removed cloud active aerosol particles, leaving the inactive components of the pollution plumes behind.

Arctic haze has traditionally been attributed to plumes of anthropogenic pollution coming from Eurasian industrial activity north of the Arctic front (Shaw, 1995). However, recent studies of large summertime Boreal forest fires in North America (Stohl et al., 2006) and Eastern European fires occurring in the Spring of 2006 (Stohl et al., 2007) arrived at the conclusion that biomass burning has been largely underestimated as a source of Arctic haze and aerosols. In fact, both anthropogenic and biomass burning pollution plumes were a primary focus of the International Polar Year (IPY) of 2007 and 2008 activities in the Arctic (Stohl, 2005). IPY field campaigns and aircraft experiments concurrent with the period of this study give a wider context for the results presented here (Ghan et al., 2007; Jacob et al., 2010).

Here, we adopt a similar approach to Avey et al. (2007) for analysis of the effects of anthropogenic and biomass burning pollution on Arctic clouds for the period 21 March through 21 July, corresponding to several IPY studies taking place during the transition

ACPD
10, 29113–29152, 2010

from the highly polluted winter to the relatively clean summer (Paris et al., 2008; Jacob et al., 2010).

2 Methods

The effect of aerosols on cloud optical depth through changes in droplet size, or the first aerosol indirect effect, is typically quantified using the Indirect Effect parameter (IE). Normally, IE is defined by the relative change in a cloud property, generally cloud optical depth (τ) or cloud droplet effective radius (r_e), with respect to a relative change in some aerosol quantity, often satellite retrieved aerosol optical depth (τ_a) (Feingold et al., 2001; Bréon et al., 2002; Lohmann and Feichter, 2005), e.g.

$$\mathrm{IE}_{r_e} = -\frac{d\ln r_e}{d\ln \tau_a} \quad (1)$$

An alternative approach is to evaluate the IE parameter with respect to fields of some passive pollution tracer that does not interact with clouds. A good choice here is Carbon Monoxide (CO) tracer concentrations produced by a Lagrangian dispersion model. Close to emission sources, anthropogenic CO generally correlates well with anthropogenic CCN in a non-precipitating air-mass (Longley et al., 2005). In the Arctic, when precipitation is low, the ratio of aerosol light scattering to short-term CO perturbations is centered around a mode value of 0.4 $\mathrm{Mm^{-1}\,ppb^{-1}}$ (Garrett et al., 2010). Unlike CCN, however, the χ_{CO} tracer is merely passive and does not interact with or influence clouds. The χ_{CO} tracer from FLEXPART is affected only by dilution up to a point of instantaneous removal at twenty days atmospheric residence time. The advantage of comparing a passive pollution tracer to cloud fields is that pollution and clouds are not coupled, for example, through wet scavenging, permitting identification of cause and effect in pollution-cloud interactions.

For example, the use of a passive tracer like χ_{CO} has the benefit of allowing information to be gathered about wet-scavenging of CCN. If concentrations of χ_{CO} are high

ACPD
10, 29113–29152, 2010

but the co-located cloud perturbations low, this may be interpreted as an indication that CCN, the cloud active components of the pollution field, have been removed through wet scavenging (Avey et al., 2007).

To explain further, assuming vertically homogenous size distributions, the cloud optical depth (τ) can be expressed as

$$\tau = \frac{3}{2}\frac{\mathrm{LWP}}{\rho_w r_e} \tag{2}$$

where ρ_w is the bulk density of liquid water, the derivative of the natural logarithm of τ with respect to the logarithm of the χ_{CO} tracer, is

$$\frac{d\ln\tau}{d\ln\chi_{CO}} = -\frac{d\ln r_e}{d\ln\chi_{CO}} + \frac{d\ln \mathrm{LWP}}{d\ln\chi_{CO}} \tag{3}$$

Since, CCN are the active components of pollution plumes, the sensitivity of cloud optical depth to pollution will be product of two partial derivatives evaluated in the following manner:

$$\frac{d\ln\tau}{d\ln\chi_{CO}} = \frac{d\ln\tau}{d\ln \mathrm{CCN}} S \tag{4}$$

where

$$S = \frac{d\ln \mathrm{CCN}}{d\ln\chi_{CO}} \tag{5}$$

is a scavenging parameter that ranges from 0 to 1 (Garrett et al., 2006, 2010). When the rate of wet scavenging is high then S will be small, indicating a small relative change in CCN for a relative change in χ_{CO}. Conversely, S is large when minimal amounts of wet scavenging have impacted the pollution plume and the correlation between CCN and χ_{CO} is high. Of course, aerosol transformations and dry deposition also contribute to the value of S, but normally such processes are relatively small (Garrett et al., 2010).

ACPD
10, 29113–29152, 2010

While cloud micro physical properties can be influenced by aerosols, they are more fundamentally determined by the meteorological conditions in which they form (Chang and Coakley, 2007). To first order, the amount of liquid water in an adiabatic cloud depends on the difference in moist and dry lapse rates at a certain temperature and pressure according to the basic thermodynamic relationship;

$$\frac{d\mathrm{LWC}}{dz} = \frac{\rho_a(T,P)C_p}{L_v}\left(\Gamma_d - \Gamma_s(T,P)\right) \quad (6)$$

where, ρ_a is the air density, C_p is the heat capacity of air, L_v the latent heat of vaporization, Γ_d the dry adiabatic lapse rate and Γ_s the moist adiabatic lapse rate. At colder temperatures the difference in lapse rates is much smaller and consequently less moisture is available for condensation and release of latent heat. For example, a cloud forming at 900 hPa at a temperature of −15 °C will have a value of $d\mathrm{LWC}/dz$ of 0.7 g m^{-3} km^{-1}. At the same height but a temperature of 0 °C, $d\mathrm{LWC}/dz$ has a value of approximately 1.9 g m^{-3} km^{-1}.

Thus, in order to limit meteorological bias and constrain cloud microphysical sensitivity to pollution, we evaluate the sensitivity of cloud properties to χ_{CO} within small bins of temperature and pressure. This minimizes covariance associated with χ_{CO} acting as a tracer of warmer, moister, airmasses that may be influencing the observed cloud properties more than pollution itself.

Furthermore, we examine only low-level, liquid clouds in the Arctic, in order to simplify interpretation of the physics and to ease comparison with prior studies that have examined the sensitivity of clouds to pollution aerosols (Garrett et al., 2004; Garrett and Zhao, 2006; Lubin and Vogelmann, 2006; Mauritsen et al., 2010). The effects of aerosols on mixed-phase clouds is a more complex issue (Curry et al., 1996; Girard et al., 2005; Morrison and Pinto, 2005; Morrison et al., 2008; de Boer et al., 2009) and not directly addressed in this study.

Here, we calculate the values of IE_{r_e}, IE_{τ}, and $\mathrm{IE}_{\mathrm{LWP}}$, by fitting a linear least squares regression of the natural logarithm of the cloud properties against the natural logarithm

ACPD
10, 29113–29152, 2010

of the combined anthropogenic and biomass burning tracers, for a given pressure level and temperature. Thus

$$\mathrm{IE}_{r_e} = -\frac{d\ln r_e}{d\ln \chi_{CO}}\bigg|_{T,P} \quad (7)$$

$$\mathrm{IE}_{\tau} = \frac{d\ln \tau}{d\ln \chi_{CO}}\bigg|_{T,P} \quad (8)$$

$$\mathrm{IE}_{LWP} = \frac{d\ln LWP}{d\ln \chi_{CO}}\bigg|_{T,P} \quad (9)$$

3 Data products used

In order to characterize pollution-cloud interactions, we use a combination of satellite retrieved cloud products and a modeled pollution tracer, as summarized in Table 1. The cloud products are retrieved using the MODIS and POLDER instruments on A-train satellites Aqua and PARASOL (Polarization and Anisotropy of Reflectances for Atmospheric Sciences coupled with Observations from a Lidar), respectively. The tracer transport model FLEXPART provides a tracer for anthropogenic emissions along with a tracer of biomass burning.

3.1 Cloud products

Aqua MODIS Collection 5 Level-2 retrievals, are used to provide cloud-top effective radius (r_e), temperature (T_C) and optical depth (τ) (Platnick et al., 2003; King et al., 2005). The retrieval of r_e is made using simultaneous measurements of cloud reflectance from the water absorbing bands (1.6, 2.1, 3.7 µm) combined with one of the non (or less) absorbing bands (0.65, 0.86, 1.2 µm) depending on the surface conditions. MODIS airborne simulator r_e values in stratiform cloud agree well with in situ measurements

ACPD
10, 29113–29152, 2010

of liquid clouds in the Arctic (Platnick et al., 2003). Cloud Liquid Water Path (LWP) is acquired from the MODIS retrieved r_e and τ parameters from Eq. (2).

Flying just two minutes behind Aqua in the A-train constellation is the microsatellite PARASOL with the innovative radiometer/polarimeter POLDER (Polarization and Directionality of the Earth's Reflectance) that provides systematic measurements of spectral, directional and polarized characteristics of reflected sunlight (Fougnie et al., 2007). This unique multidirectional instrument provides cloud microphysical and macrophysical parameters at a spatial resolution close to 20 km × 20 km.

Here, cloud pressure is determined from the POLDER cloud oxygen pressure (P_{O_2}), which is based on the differential absorption measured at 763 and 765 nm wavelength, corresponding to the A-band region of strong absorption by atmospheric oxygen (Bréon and Colzy, 1999). Multiple scattering in cloud places P_{O_2} values more towards the center of the cloud rather than cloud top. Nonetheless, P_{O_2} cloud top pressure from POLDER is preferred over MODIS cloud top pressure retrievals because the P_{O_2} algorithm does not utilize infrared channels that require an assumed temperature profile (Buriez et al., 1997; Weisz et al., 2007). Thus, it is unaffected by the presence of surface temperature inversions, which can be common in the Arctic (Shupe et al., 2006) and affect MODIS cloud top height retrievals in marine subtropical regions (Holz et al., 2008). Described in Sect. 3.3, we find that for low-level clouds in the Arctic, MODIS cloud heights can be several kilometers too high.

With respect to detection of cloud phase, angular polarization features of shortwave radiation reflected off clouds depend strongly on particle shape and POLDER captures a polarization signature unique to water droplets but absent in ice (Goloub et al., 2000). One of the MODIS phase retrievals makes use of the strong differences in the spectral absorption characteristics of ice and water in the 8.5 µm and 11 µm radiation bands (Platnick et al., 2003). An additional MODIS phase retrieval uses measurements of shortwave infrared reflectance (SWIR) at the wavelengths 1.6 and 2.1 µm and reflectance in the visible channels (King et al., 2003), taking advantage of the fact that ice particles are slightly more absorbing at SWIR wavelengths than liquid water

ACPD
10, 29113–29152, 2010

droplets. While each retrieval has it's own set of advantages and limitations, the A-train allows the POLDER and MODIS products to be combined synergistically to provide a semi-continuous confidence index for thermodynamic phase (ϕ) ranging from confident liquid (1) to confident ice (200) (Riedi et al., 2007).

Here, clouds with a value of ϕ that is 50 or below are assumed to be liquid because it requires that at least two of the three retrieval algorithms used in the index agree on phase determination.

3.2 Anthropogenic and biomass burning pollution tracer

The Lagrangian particle dispersion model FLEXPART (Stohl et al., 2005) is used here to characterize the transport of pollution into the Arctic, represented by CO concentrations fields (χ_{CO}) from recent (<20 days old) anthropogenic combustion and biomass burning emissions. The model is driven by the European Centre for Medium Range Weather Forecasts operational analyses (White, 2002) and produces pollution tracer output at 15 tropospheric vertical model levels, with a global horizontal resolution of $0.5^{\circ} \times 0.5^{\circ}$ in three hour time steps. FLEXPART calculates the trajectories of tracer particles using the mean winds interpolated from the meteorological analysis fields plus parametrized random motions representing turbulence and convection (Stohl and Thomson, 1999).

Anthropogenic emission sources are calculated from the EDGAR emission inventory outside North America (Olivier and Berdowski, 2001). For North America, emissions were calculated using the inventory by Frost et al. (2006). A tracer of biomass burning is incorporated into the model based on a fire detection scheme from the MODIS instruments on Aqua and Terra (Giglio et al., 2003) and using an algorithm described by Stohl et al. (2007). The FLEXPART model has been a popular choice for understanding the origins and characteristics of Arctic air pollution (Stohl et al., 2007; Law and Stohl, 2007; Stohl, 2006). During the IPY airborne field experiments, ARCTAS (Arctic Research of the Composition of the Troposphere from Aircraft and Satellites) and

ACPD
10, 29113–29152, 2010

ARCPAC (Aerosol, Radiation, and Cloud Processes affecting Arctic Climate), FLEXPART was used to predict locations of pollution plumes in order to select appropriate flight plans for in situ pollution measurements (Fuelberg et al., 2010; Jacob et al., 2010). Not only were pollution plume locations accurate, predicted CO enhancements also agreed well with coincident airborne measurements (Warneke et al., 2010).

3.3 Co-location of cloud products with FLEXPART

Here, we examine the entire Arctic region between 65° N and 84° N, subject to satellite retrieval constraints. The orientation of the polar orbiting satellites means that the largest sampling density (approximately 42%) lies between 70° N and 75° N, including a large portion of land mass, some sea ice in the early part of the study and later open ocean.

Satellite retrieved cloud properties from POLDER and MODIS are provided at different spatial resolutions. For a nadir view, MODIS cloud products are provided at 1 km × 1 km resolution for τ and r_e, while T_C is provided at 5 km × 5 km resolution. The POLDER P_{O_2} pressure is derived from 6 km × 6 km resolution observations but it is provided at a fixed resolution of 20 km × 20 km. The synergistic POLDER-MODIS cloud phase product is derived and provided at the full POLDER native resolution of 6 km × 6 km.

Prior to co-location with the FLEXPART tracer fields, all satellite cloud products are spatially co-located on a fixed resolution sinusoidal grid (equal area) of 6 km × 6 km to maintain phase information at its highest resolution. Next, these merged POLDER and MODIS cloud products are temporally and spatially co-located with FLEXPART output. We match the A-train satellite overpass time to the appropriate FLEXPART tracer field, which is output every three hours. For example, a 08:33 UTC satellite overpass will be matched up with the 09:00 UTC FLEXPART pollution tracer fields, which represent an average of tracer concentrations between 06:00 and 09:00 UTC for that particular grid cell.

ACPD
10, 29113–29152, 2010

Establishing the vertical location of both aerosols and clouds is the best way to determine if the two quantities are interacting on a microphysical level consistent with the aerosol indirect effect. For clouds forming in the tropical and subtropical marine boundary layer, the MODIS operational Collection Five cloud top pressure retrieval has been known to overestimate cloud top heights by 1 to 3 km (Holz et al., 2008). This bias is likely a result of problems the algorithm has in matching the observed 11 µm brightness temperature to a unique atmospheric level in the presence of a strong subsidence temperature inversion. If a bias this large is similarly present in Arctic low-level cloud measurements, the ability to diagnose aerosol-cloud interactions using our analysis technique would be seriously compromised when using MODIS cloud top height retrievals. The Arctic is not subject to the same large scale subsidence of subtropical regions. However, strong temperature inversions are often present (Shupe et al., 2006), possibly affecting MODIS cloud top height retrievals.

The synergy of the A-train satellite group allows retrievals from different active and passive instruments to be meaningfully compared. As an alternative to the MODIS instrument, the POLDER cloud top height algorithm offers a very similar footprint and spatial resolution, but it uses measurements from visible rather than infrared wavelength channels (Bréon and Colzy, 1999), eliminating the need for an estimated temperature profile in cloud placement determination.

We performed an inter-comparison of MODIS, POLDER and CALIOP cloud top heights in order to determine whether a bias affecting MODIS cloud top height retrievals of Arctic low-level clouds was present and if utilizing in it's place, the POLDER algorithm offered any improvement. Cloud top heights from the three instruments were compared for multiple scenes of low-level stratiform clouds forming in the Arctic region spanning April to July, 2008. Figure 1 shows an example of MODIS, POLDER and CALIOP cloud top height retrievals co-located along the CALIOP footprint plotted with the vertical profile of modeled biomass burning and anthropogenic pollution tracer output. MODIS cloud top heights correspond to pollution tracer concentrations that are considerably different than the layer where the CALIOP Lidar and POLDER cloud

ACPD
10, 29113–29152, 2010

top height retrievals indicate the cloud actually lies. For the low-level Arctic stratiform clouds that were compared, MODIS cloud top heights were found to have a consistent positive bias of 1.6 ± 0.5 km compared to POLDER and CALIOP.

The scheme for horizontal and vertical co-location is illustrated in Figs. 2 and 3. FLEXPART concentrations are output for atmospheric layers of roughly 1 km depth in the lower troposphere. Cloud retrievals associated with POLDER P_{O_2} pressures lying within the boundaries of each FLEXPART grid box are compared with the FLEXPART concentrations in that grid box. Clouds with P_{O_2} pressures between 800 hPa and 900 hPa are co-located with FLEXPART concentrations for FLEXPART grid boxes between 1 km and 2 km; clouds with P_{O_2} pressures between 900 hPa and 975 hPa are co-located with FLEXPART concentrations for the grid boxes between 200 m and 1 km.

The $0.5^\circ \times 0.5^\circ$ horizontal resolution of the FLEXPART model grid is considerably coarser than the 6 km × 6 km satellite derived cloud property retrievals. To account for this difference in resolution, an averaging of cloud properties is performed for each FLEXPART three dimensional grid box such that each grid box has only one set of cloud property values associated with it. Within each FLEXPART grid box, satellite retrieved properties are averaged together only if all retrievals of the considered cloud properties are successful. For example, if a cloud pixel has a successful cloud top height and effective radius retrieval, but the thermodynamic phase is undetermined, then none of the properties from that pixel are included in the analysis.

For the atmospheric heights below 800 hPa used in this study, clouds are generally stratiform so that within a typical FLEXPART grid box, the variability in cloud properties is relatively small. Grid boxes with less than 50% cloud coverage within a given FLEXPART level were not used in the assessment of pollution-cloud interactions.

The co-location method is subject to some amount of error and uncertainty that will affect the relationships between χ_{CO} and cloud properties. FLEXPART χ_{CO} fields are only output every three hours, meaning that the maximum temporal difference between observed cloud properties and the pollution tracer is 1.5 h. Advection errors from the ECMWF model grids and parametrized turbulence are also possible. Anthropogenic

ACPD
10, 29113–29152, 2010

emission inventories are based on data from previous years, which makes χ_{CO} emission estimations another source of uncertainty. Furthermore, MODIS is only able to detect biomass burning under relatively cloud free conditions, possibly leading to underpredicted biomass burning χ_{CO}.

The advantage of co-locating satellite and FLEXPART fields is that it allows for high statistical coverage of the Arctic while allowing for comparison of pollution and clouds under similar meteorological regimes.

4 Observations

Figure 4 illustrates the general nature of the liquid clouds that were analyzed over the period between 20 March and 20 July 2008. More than 80% had cloud top temperatures below freezing, indicating supercooled water droplets. The characteristics of the retrieved cloud properties are, for the most part, consistent with prior in-situ measurements of Arctic stratiform clouds (Curry et al., 1996; Shupe et al., 2006; de Boer et al., 2009). For clouds between 800 hPa and 900 hPa, median [lower quartile, upper quartile] values for τ are 11.4 [6.9, 17.1], 82.7 $\mathrm{g\,m^{-2}}$ [49.6, 128.2] for LWP and 10.8 µm [8.94, 13.33] for r_e and for clouds between 900 hPa and 975 hPa values are τ 10.0 [6.6 14.5] for τ, 69 $\mathrm{g\,m^{-2}}$ [41.7, 107.3] for LWP and 9.9 µm [8.3, 11.9] for r_e.

Figure 5 shows an example of the calculation of IE_{r_e} (Eq. 7), showing a comparison between FLEXPART χ_{CO} fields and space-based retrievals of retrievals of r_e in low-level liquid clouds. It is clear from the scatter in this figure that pollution is not the primary control of cloud effective radius. Meteorology almost certainly plays a larger role. However, with sufficient statistics it is nonetheless apparent that there is a weak correlation between high levels of pollution and small effective radii.

Figure 6 shows the IE parameter (Eqs. 7–9) calculated for small bins (2 °C) of cloud top temperature T_C and pressure for clouds with any retrieved value of LWP. As an additional constraint, Fig. 6 also shows the IE parameter calculated for clouds with LWP $<40\,\mathrm{g\,m^{-2}}$ and LWP $>40\,\mathrm{g\,m^{-2}}$. The value of LWP $<40\,\mathrm{g\,m^{-2}}$ is chosen in order to

ACPD
10, 29113–29152, 2010

isolate any dynamic feedbacks in clouds that may occur in clouds that are sufficiently thin to act as graybody emitters (Garrett et al., 2002). Clouds emitting as graybodies are hypothesized to be particularly susceptible to aerosol enhancements that create a climatologically significant warming effect (Garrett and Zhao, 2006; Lubin and Vogelmann, 2006; Mauritsen et al., 2010), and reductions in droplet effective radius can accelerate their development through a radiative-dynamic feedback mechanism (Garrett et al., 2009). Once the LWP exceeds 40 gm^{-2} the cloud is an approximate blackbody and cloud longwave emission is determined by temperature changes alone.

The plots show that independent of pressure level, there is a general increase in values of IE with temperature until T_C reach 0 °C , and lower sensitivity at higher temperatures. Except for the coldest temperatures (< −8 °C), the sensitivity is larger for τ than for r_e because changes in χ_{CO} are also associated with changes in LWP. Values of IE are smaller for graybody clouds with LWP < 40 gm^{-2} than they are for thicker clouds.

For the span of this study, we find that biomass burning is clearly affecting the composition of the Arctic lower troposphere, contributing to approximately half of the χ_{CO} concentrations coincident with the clouds that were sampled independent of potential temperature Fig. 7 shows a clear association between larger values of χ_{CO} and warmer potential temperatures (θ), where $\theta = T(P_0/P)^{2/7}$ and $P_0 = 1000$ hPa. This is expected as most pollution originates from lower latitudes and is transported roughly isentropically into the Arctic (Stohl, 2006). For the low level Arctic clouds analyzed, the ratio of anthropogenic χ_{CO} to χ_{CO} from biomass burning is near unity, independent of potential temperature.

Here, the chemical composition and relative amounts of ΔCCN for the different tracers are unknown and will influence the sensitivity of cloud properties to χ_{CO}. Prior studies suggest that the quantity of CCN per unit CO in pollution plumes is somewhat sensitive to whether the origins are from biomass burning or anthropogenic combustion. For example, from in-situ measurements made near industrial mid-latitude sites in North America and Europe, the ratio of ΔCCN/ΔCO is roughly 25 ± 15 cm^{-3} ppb^{-1} (Longley et al., 2005; Garrett et al., 2006). Comparable values of 40 ± 20 cm^{-3} ppb^{-1} can be

ACPD
10, 29113–29152, 2010

computed for Arctic haze by relating observed ratios of droplet number concentrations to aerosol light scattering (σ), which are $100 \pm 50\,\mathrm{cm}^{-3}\,\mathrm{Mm}^{-1}$ (Garrett et al., 2004), to observations from the same location of $\Delta\sigma/\Delta\mathrm{CO}$, which are $0.4 \pm 0.1\,\mathrm{Mm\,ppb}^{-1}$ (Garrett et al., 2010). Estimating values for the ratio $\Delta\mathrm{CCN}/\chi_{\mathrm{CO}}$ in biomass burning is more difficult because fuel type and fire size play a large role in the aerosol mass concentration and solubility (Rivera-Carpio et al., 1996; Reid et al., 2005). Large Siberian Boreal forest fires are a major but episodic source of aerosols during the spring and summer (Stohl, 2006). Unfortunately, this remote region is lacks studies of CCN emission characteristics (Paris et al., 2008). While regionally distinct, the scale and scope of Siberian Boreal forest fires are nonetheless similar to large tropical fires (Andreae et al., 2004; Vestin et al., 2007), where $\Delta\mathrm{CCN}/\Delta\mathrm{CO}$ values of $10 \pm 2\,\mathrm{cm}^{-3}$ ppb^{-1} were observed.

This suggests that $\Delta\mathrm{CCN}/\chi_{\mathrm{CO}}$ is potentially a factor of two (or more) larger for the anthropogenic tracer than it is for biomass burning plumes. To examine the sensitivity of clouds to differing pollution sources, we calculate values of IE for clouds where FLEXPART biomass burning χ_{CO} concentrations were either >80% or <20% of the total χ_{CO} concentrations (Fig. 8).

Figure 8 shows that when biomass burning χ_{CO} concentrations are relatively high, Arctic cloud properties show a sensitivity to pollution plumes that can be significant, particularly along isentropic surfaces between 282 K and 291 K. Overall, however, biomass pollution plumes have a smaller effect on cloud properties per unit CO than do anthropogenic plumes.

5 Discussion

5.1 Overall low-level Arctic cloud response to pollution plumes

Calculated for low-level, liquid, stratiform clouds, north of 65° N Latitude, from the end of March through mid-July 2008, we obtain values for the IE parameter calculated with respect to a pollution tracer that range from 0.00 to 0.10 with respect to effective radius

ACPD
10, 29113–29152, 2010

(r_e) and values of 0.00 to 0.21 with respect to optical depth (τ), with the largest values at temperatures near freezing.

For comparison, using ground based measurements obtained near Barrow Alaska, Garrett et al. (2004) found values of IE_{r_e} for low-level liquid clouds in the range of 0.13 to 0.19 when the aerosol quantity considered was light scattering of sub-micron aerosol. Lihavainen et al. (2009) found IE_{r_e} values of 0.2 to 0.3 in ground based measurements in Northern Finland and values of ~ 0.1 in satellite measurements for both IE_{r_e} and IE_{τ}.

More globally, satellite based studies have obtained IE values ranging from 0.02 to 0.20 for continental clouds (Nakajima et al., 2001; Feingold et al., 2003; Lohmann and Feichter, 2005; Myhre et al., 2007) and 0.09 to 0.13 for oceanic clouds (Bréon et al., 2002; Sekiguchi et al., 2003; Kaufman et al., 2005; Myhre et al., 2007). Costantino and Bréon (2010) used space-based lidar to determine that African biomass burning aerosol layers that were likely coincident and interacting with shallow marine stratocumulus clouds had IE values of 0.24. However, if there was no indication that aerosol layers were coincident with clouds, the IE value fell to 0.04, demonstrating the importance of vertical and horizontal co-location of aerosol and cloud in studies of the aerosol indirect effect.

Our analysis technique made many efforts to ensure clouds are compared with coincident pollution. However, limitations and uncertainties with the co-location technique, combined with advection errors in modeled FLEXPART pollution levels, will act to reduce the correlation between cloud properties and χ_{CO}, leading to smaller values of IE.

Overall, the values of IE we calculated are smaller than prior ground-based studies that directly compared coincident clouds and aerosols. This may be due in part to co-location errors in the comparisons between satellite-retrieved cloud properties and pollution fields from FLEXPART. More importantly, however, comparisons were not made with respect to an aerosol quantity but rather to a passive pollution tracer χ_{CO}. Since concentrations of χ_{CO} are independent of clouds and only affected by dilution and mixing, when the IE parameter is large the implication is that values of the scavenging

ACPD
10, 29113–29152, 2010

parameter, S (Eq. 5) are close to unity and pollution plumes are associated with significant concentrations of CCN that have the capacity to perturb cloud properties. It is no surprise then that the largest values of IE that we see are similar to those obtained in previous studies. However, we find that frequently values of IE (and S) are quite small, particularly when T_C is greater than 4 °C. This suggests that at very warm temperatures wet scavenging is sufficiently efficient to limit the effects of pollution plumes on cloud properties. CCN are efficiently removed, leaving behind pollution tracers that are inactive with respect to clouds. Perhaps the freezing point serves as a "scavenging point" (Garrett et al., 2010) because warm rain collision-coalescence mechanisms can combine millions of CCN into a single raindrop.

What is a bit surprising is that there appears to be lowered sensitivity of clouds to pollution plumes at locally cold temperatures below −6 °C or below potential temperatures of about 278 K. It is unclear why this should be so given that wet scavenging is unlikely to be particularly efficient due to low precipitation rates. Perhaps one explanation is that cold air masses are also associated with longer transport times from mid-latitude pollution source regions (Stohl, 2006). It is the time-integral of precipitation rates that ultimately determines the extent of wet scavenging. It may be that the "inverted-U" shape in the IE signature appears due to two competing effects: precipitation is low but transport times are long along cold potential temperature surfaces; conversely, transport times are short but precipitation is high along warm potential temperature surfaces. Values of IE are at a maximum for temperatures where the time integral of precipitation rates along transport pathways is at a minimum.

The broad statistical nature of the data sampling allows for the effects of possible dynamical and microphysical feedback processes to be evident in the analyses. Our dataset encompasses a broad time period and samples clouds at various points from their formation all the way until dissipation. Any feedback mechanisms occurring on short time scales will also be contributing to our results. If LWP is unaffected by pollution and S is low, then the IE parameter calculated with respect to r_e and τ will be equal (see Eq. 3), and absent any dynamical feedbacks, IE values will range between 0 and

ACPD
10, 29113–29152, 2010

0.33 (Feingold, 2003). Here, we allow for feedbacks that would increase LWP and are usually neglected in aerosol indirect effect studies (Stevens and Feingold, 2009), the idea being that we are empirically fitting a slope to data that encompasses many phenomena in a complex system. Our data sampling occurs at various stages of a cloud's lifetime and over a long time period, so the results will include information about any dynamical feedback or precipitation process that may mediate the overall cloud response to pollution.

Figure 9 shows observed values of an enhancement factor (EF) representing the degree to which the cloud optical depth sensitivity IE_τ exceeds the droplet effective radius sensitivity IE_{r_e} based on results in shown in Fig. 5, and plotted against potential temperature. When no constraint is made on LWP, values of EF are about four for values of θ >273 K. The magnitude of the enhancement factor is smaller by about a factor of two when LWP is constrained to graybody clouds or blackbody clouds and for periods when biomass burning is greater than 80% total χ_{CO} .

Thus, our results suggest that LWP in Arctic low-level liquid clouds is more sensitive to mid-latitude pollution plumes than is r_e. This is surprising given that the most simple understanding of cloud physics is that values of LWP are determined primarily by thermodynamic constraints rather than aerosol concentrations. We cannot isolate an exact physical mechanism from the observations. One possibility, though, is that enhancement at low LWP may be indicative of a infrared radiative feedback process that accelerates cloud development when clouds are thin and polluted (Garrett et al., 2009). Alternatively, suppression of warm rain and drizzle by pollution aerosol may lead to a long term thickening of liquid stratiform clouds (Pincus and Baker, 1994; Wood, 2007; Stevens and Feingold, 2009).

Also, a common but tenuous regime of supercooled liquid clouds precipitating ice, is frequently observed in the Arctic (Curry et al., 1996; Intrieri et al., 2002; Shupe et al., 2006). Morrison et al. (2008) found in model simulations that elevated aerosol concentrations reduce riming processes in Arctic clouds and this can lead to increased LWP and cloud lifetime because ice particle growth is inhibited and suppresses ice crystal

ACPD
10, 29113–29152, 2010

precipitation. By restricting our analysis to clouds with a radiatively determined phase index of $\phi < 50$, our study likely did not exclude liquid clouds that were precipitating ice. Thus, this feedback potentially is contributing to our observation of LWP sensitivity to pollution, even if it would not explain large enhancement values (EF) at high temperatures (Fig. 9).

A correlation between χ_{CO} and LWP may also be expected for dynamical reasons. As a polluted, warm, mid-latitude air mass intrudes into the Arctic, it typically rises slantwise along a frontal surface above the colder Arctic dome. A cloud forming in such an air mass might be expected to be deeper than an average Arctic cloud considered in our analysis. The impact on our results is minimized by controlling our analyses for both cloud top temperature and pressure and considering only stratiform clouds with cloud tops below 2 km, whose depth is clearly limited. Still, the effect may partly explain why IE_{LWP} values are larger than IE_{r_e} values.

Further explanation for the observed sensitivity of LWP to the pollution tracer χ_{CO} warrants further investigation. Perhaps, sensitivity studies using LES (Large Eddy Simulation) type cloud models may provide better insight into interpreting our observations. Similarly, if precipitation observations could be coupled with our cloud property observations, a more precise understanding of pollution-cloud interactions could be achieved, since precipitation determines wet scavenging and is closely tied to cloud microphysical properties.

5.2 Cloud response to biomass burning

Natural and anthropogenic aerosol sources may have the capacity to influence cloud properties (Quinn et al., 2008; Hirdman et al., 2010). However, the bulk of Arctic aerosol mass originates from outside the Arctic (Sirois and Barrie, 1999; Law and Stohl, 2007) and is well represented in FLEXPART by the anthropogenic and biomass burning tracers χ_{CO}.

Figure 7 indicates that biomass burning contributes significantly to total pollution levels affecting low-level liquid clouds in the Arctic, consistent with results from several

ACPD
10, 29113–29152, 2010

ARCPAC and ARCTAS related studies during April and July 2008 (Fuelberg et al., 2010). Unusually warm temperatures and reduced snow cover in the early spring favored pollution transport into the Arctic from Siberian wildfires and Kazakhstan agricultural burning (Warneke et al., 2009, 2010). Later in the summer, frequent biomass burning plumes were observed, often in elevated layers that originated from eastern Siberian wildfires (Paris et al., 2008; Fuelberg et al., 2010).

We find that, compared to when anthropogenic pollution dominates the plumes, plumes dominated by biomass burning exhibit a generally smaller response of cloud optical depth to pollution (Fig. 9). The LWP response is near zero. One reason may be that biomass burning pollution plumes contain a smaller proportion of highly soluble CCN per unit CO than anthropogenic plumes. Biomass burning plumes typically contain CCN that are a mixture of soluble and insoluble particles activating at a much larger range of supersaturations (Rivera-Carpio et al., 1996; Pradeep Kumar et al., 2003; Vestin et al., 2007).

The minimal enhancement in values of IE_{τ} over IE_{r_e} (Fig. 9) observed in biomass burning dominated pollution plumes and may point to other radiative characteristics of biomass burning aerosols dampening feedback processes affecting LWP in anthropogenic dominated plumes. For instance, our study did not preclude situations where additional biomass burning layers may be situated above the cloud layer. During the late spring and summer these layers would strongly absorb shortwave radiation and add an additional thermal forcing at cloud top (Brioude et al., 2009). The added warm layer may increase the atmospheric stability and favor low cloud development or conversely, the added thermal flux may decrease the relative humidity and enhance evaporation, dissipating the cloud (Klein and Hartmann, 1993). While, we show an overall sensitivity of cloud properties to biomass burning plumes, a closer examination of the vertical profile and thermal characteristics of the biomass burning tracer is needed in order to constrain these possible effects.

ACPD
10, 29113–29152, 2010

6 Conclusions

This study has shown how an inert passive tracer can be used to quantify the indirect effects of anthropogenic and biomass burning pollution plumes on the properties of low-level liquid clouds in the Arctic north of 65°. Results show that, for a fairly narrow range of temperatures, the effects of pollution plumes on clouds is of a similar magnitude to those seen in previous satellite studies that looked explicitly at the effects of measured aerosols on clouds. The highest correlation between cloud optical depth, droplet effective radius and pollution occurs at temperatures near freezing.

However, there is a pronounced decrease in the sensitivity of clouds to pollution plumes at temperatures that are both warmer and colder than freezing, or alternatively potential temperatures that are warmer or colder than about 286 K. We suggest that an explanation for this "inverted-U" phenomenon is the extent of time-integrated wet scavenging of aerosols along transport pathways from mid-latitudes. At warmer temperatures, the decrease is due to more efficient wet scavenging of CCN in seasonally warm and moist air-masses. At colder temperatures, the transport time to the Arctic of air from mid-latitudes is prolonged, and this increases potential exposure to precipitation events.

We find also that biomass burning plumes interact less efficiently with clouds, per unit CO, than do anthropogenic plumes, although their effects are still significant. Finally, independent of temperature, we find that the cloud optical depth has a substantially higher sensitivity to changes in pollution levels, typically by a factor of four, than can be explained by changes in cloud droplet effective radius alone. What this suggests is that pollution aerosols are activating precipitation suppression or some unknown dynamic feedback mechanism to increase liquid water path and cause large enhancements of the first indirect effect of aerosols on low-level Arctic liquid clouds.

Acknowledgements. This work was supported through National Science Foundation award ATM0649570 to TJG.

ACPD
10, 29113–29152, 2010

References

Ackerman, A. S., Kirkpatrick, M. P., Stevens, D. E., and Toon, O. B.: The impact of humidity above stratiform clouds on indirect aerosol climate forcing, Nature, 432, 1014–1017, doi:10.1038/nature03174, 2004. 29115

Albrecht, B.: Aerosols, cloud microphysics and fractional cloudiness, Science, 245, 1227–1230, doi:10.1126/science.245.4923.1227, 1989. 29115

Andreae, M. O., Rosenfeld, D., Artaxo, P., Costa, A., Frank, G. P., and Longo, K. M.: Smoking Rain Clouds over the Amazon, Science, 303, 1337–1342, doi:10.1126/science.1092779, 2004. 29128

Avey, L., Garrett, T., and Stohl, A.: Evaluation of the aerosol indirect effect using satellite, tracer transport model, and aircraft data from the International Consortium for Atmospheric Research on Transport and Transformation, J. Geophys. Res., 112, doi:10.1029/2006JD007581, 2007. 29116, 29118

Bréon, F., Tanré, D., and Generoso, S.: Aerosol effect on cloud droplet size monitored from satellite, Science, 295, 834–838, doi:10.1126/science.1066434, 2002. 29117, 29129

Bréon, F. M. and Colzy, S.: Cloud detection from spaceborne POLDER instrument and validation against surface synoptic observations, J. Appl. Meteorol., 36, 777–785, doi:10.1175/1520-0450, 1999. 29121, 29124

Brioude, J., Cooper, O. R., Feingold, G., Trainer, M., Freitas, S. R., Kowal, D., Ayers, J. K., Prins, E., Minnis, P., McKeen, S. A., Frost, G. J., and Hsie, E.-Y.: Effect of biomass burning on marine stratocumulus clouds off the California coast, Atmos. Chem. Phys., 9, 8841–8856, doi:10.5194/acp-9-8841-2009, 2009. 29116, 29133

Buriez, J. C., Vanbauce, C., Parol, F., Goloub, P., Herman, M., Bonnel, B., Fouquart, Y., Couvert, P., and Seze, G.: Cloud detection and derivation of cloud properties from POLDER, Int. J. Remote Sens., 18, 2785–2813, doi:10.1080/014311697217332, 1997. 29121

Chang, F. and Coakley, J. A.: Relationships between Marine Stratus Cloud Optical Depth and Temperature Inferences from AVHRR Observations, J. Climate, 20, 2022–2036, doi:10.1175/JCLI4115.1, 2007. 29119

Costantino, L. and Bréon, F. M.: Analysis of aerosol-cloud interaction from multi-sensor satellite observations, Geophys. Res. Lett., 37, L11801, doi:10.1029/2009GL041828, 2010. 29129

Curry, J., Rossow, W., and Randall, D.: Overview of Arctic Cloud and Radiation Characteristics., J. Climate, 9, 1731–1764, doi:10.1175/1520-0442(1996)009⟨1731:OOACAR⟩2.0.CO;2,

ACPD
10, 29113–29152, 2010

1996. 29119, 29126, 29131
de Boer, G., Eloranta, E. W., and Shupe, M. D.: Arctic Mixed-Phase Stratiform Cloud Properties from Multiple Years of Surface-Based Measurements at Two High-Latitude Locations, J. Atmos. Sci., 66, 2874–2887, doi:10.1175/2009JAS3029.1, 2009. 29119, 29126
Durkee, P. A., Noone, K. J., Ferek, R. J., Johnson, D. W., Taylor, J. P., Garrett, T. J., Hobbs, P. V., Hudson, J. G., Bretherton, C. S., Innis, G., Frick, G. M., Hoppel, W. A., AoDowd, C. D., Russell, L. M., Gasparovic, R., Nielsen, K. E., Tessmer, S. A., Osborne, S. R., Flagan, R. C., Seinfeld, J. H., and Rand, H.: The Impact of Ship-Produced Aerosols on the Microstructure and Albedo of Warm Marine Stratocumulus Clouds: A Test of MAST Hypotheses 1 and 2, J. Atmos. Sci., 57, 2554–2569, doi:10.1175/1520-0469(2000)057⟨2554:TIOSPA⟩2.0.CO;2, 2000. 29115
Feingold, G.: Modeling of the first indirect effect: Analysis of measurement requirements, Geophys. Res. Lett., 30, L1997, doi:10.1029/2003GL017967, 2003. 29131
Feingold, G., Remer, L. A., Ramaprasad, J., and Kaufman, Y. J.: Analysis of smoke impact on clouds in Brazilian biomass burning regions: An extension of Twomey's approach, J. Geophys. Res., 106, 22907–22922, doi:10.1029/2001JD000732, 2001. 29117
Feingold, G., Eberhand, W., and Veron, D. E.: First measurements of the Twomey indirect effect using ground based remote sensors., Geophys. Res. Lett., 30, L1287, doi:10.1029/2002GL016633, 2003. 29129
Fougnie, B., Bracco, G., Lafrance, B., Ruffel, C., Hagolle, O., and Tinel, C.: PARASOL in-flight calibration and performance, Appl. Optics, 46, 5435–5451, doi:10.1364/AO.46.005435, 2007. 29121, 29143
Frost, G. J., McKeen, S. A., Trainer, M., Ryerson, T. B., Neuman, J. A., Roberts, J. M., Swanson, A., Holloway, J. S., Sueper, D. T., Fortin, T., Parrish, D. D., Fehsenfeld, F. C., Flocke, F., Peckham, S. E., Grell, G. A., Kowal, D., Cartwright, J., Auerbach, N., and Habermann, T.: Effects of changing power plant NO_x emissions on ozone in the eastern United States: Proof of concept, J. Geophys. Res., 111, D12306, doi:10.1029/2005JD006354, 2006. 29122
Fuelberg, H. E., Harrigan, D. L., and Sessions, W.: A meteorological overview of the ARCTAS 2008 mission, Atmos. Chem. Phys., 10, 817–842, doi:10.5194/acp-10-817-2010, 2010. 29123, 29133
Garrett, T. J. and Zhao, C.: Increased Arctic cloud longwave emissivity associated with pollution from mid-latitudes, Nature, 440, 787–789, doi:10.1038/nature04636, 2006. 29115, 29119, 29127

ACPD
10, 29113–29152, 2010

Garrett, T. J., Radke, L. F., and Hobbs, P. V.: Aerosol Effects on Cloud Emissivity and Surface Longwave Heating in the Arctic., J. Atmos. Sci., 59, 769–778, doi:10.1175/1520-0469(2002)059, 2002. 29115, 29127

Garrett, T. J., Zhao, C., Dong., X., Mace, G. G., and Hobbs, P. V.: Effects of varying aerosol regimes on low-level Arctic stratus, Geophys. Res. Lett., 31, L17105, doi:10.1029/2004GL019928, 2004. 29119, 29128, 29129

Garrett, T. J., Avey, L., Palmer, P. I., Stohl, A., Neuman, J. A., Brock, C. A., Ryerson, T., and Holloway, J. S.: Quantifying wet scavenging processes in aircraft observations of nitric acid and CCN, J. Geophys. Res., 111, D23S51, doi:10.1029/2006JD007416, 2006. 29118, 29127

Garrett, T. J., Maestas, M. M., Kruegar, S. K., and Schmidt, C. T.: Acceleration of a radiative-thermodynamic cloud feedback influencing Arctic surface warming, Geophys. Res. Lett., 36, L19804, doi:10.1029/2009GL040195, 2009. 29127, 29131

Garrett, T. J., Zhao, C., and Novelli, P.: Assessing the relative contributions of transport efficiency and scavenging to seasonal variability in Arctic aerosol, Tellus B., 62, 190–196, doi:10.1111/j.1600-0889.2010.00453.x, 2010. 29114, 29117, 29118, 29128, 29130

Ghan, S., Schmid, B., Hubbe, J., Flynn, C., Laskin, A., Zelenyuk, D., Czizco, D., and Long, C. N.: Science Overview Document Indirect and Semi-Direct Aerosol Campaign (ISDAC) April 2008, Tech. rep., U.S. Department of Energy, 2007. 29116

Giglio, L., Descloitres, J., Justice, C. O., and Kaufman, Y. J.: An Enhanced Contextual Fire Detection Algorithm for MODIS, Remote Sens. Environ., 87, 273–282, doi:10.1016/S0034-4257(03)00184-6, 2003. 29122

Girard, E., Blanchet, J.-P., and Dubois, Y.: Effects of arctic sulphuric acid aerosols on wintertime low-level atmospheric ice crystals, humidity and temperature at Alert, Nunavut, Atmos. Res., 73, 131–148, doi:10.1016/j.atmosres.2004.08.002, 2005. 29119

Goloub, P., Herman, M., Chepfer, H., Riedi, J., Brogniez, G., Couvert, P., and Seze, G.: Cloud thermodynamical phase classification from the POLDER spaceborne instrument, J. Geophys. Res., 105, 14747–14760, doi:10.1029/1999JD901183, 2000. 29121

Hirdman, D., Sodemann, H., Eckhardt, S., Burkhart, J. F., Jefferson, A., Mefford, T., Quinn, P. K., Sharma, S., Ström, J., and Stohl, A.: Source identification of short-lived air pollutants in the Arctic using statistical analysis of measurement data and particle dispersion model output, Atmos. Chem. Phys., 10, 669–693, doi:10.5194/acp-10-669-2010, 2010. 29132

Hobbs, P. V., Garrett, T. J., Ferek, R. J., Strader, S. R., Hegg, D. A., Frick, G. M., Hoppel, W. A., Gasparovic, R. F., Russell, L. M., Johnson, D. W., O'Dowd, C., Durkee, P. A., Nielsen, K. E.,

ACPD
10, 29113–29152, 2010

and Innis, G.: Emissions from Ships with respect to Their Effects on Clouds, J. Atmos. Sci., 57, 2570–2590, doi:10.1175/1520-0469(2000)057⟨2570:EFSWRT⟩2.0.CO;2, 2000. 29115
Holz, R. E., Ackerman, S. A., Nagle, F. W., Frey, R., Dutcher, S., Kuehn, R. E., Vaughan, M. A., and Baum, B.: Global Moderate Resolution Imaging Spectroradiometer (MODIS) cloud detection and height evaluation using CALIOP, J. Geophys. Res., 113, D00A19, doi:10.1029/2008JD009837, 2008. 29121, 29124
Intrieri, J. M., Fairall, C. W., Shupe, M. D., Persson, P. O. G., Andreas, E. L., Guest, P. S., and Moritz, R. E.: An annual cycle of Arctic surface forcing at SHEBA, J. Geophys. Res., 107, C8039, 2002. 29131
Jacob, D. J., Crawford, J. H., Maring, H., Clarke, A. D., Dibb, J. E., Emmons, L. K., Ferrare, R. A., Hostetler, C. A., Russell, P. B., Singh, H. B., Thompson, A. M., Shaw, G. E., McCauley, E., Pederson, J. R., and Fisher, J. A.: The Arctic Research of the Composition of the Troposphere from Aircraft and Satellites (ARCTAS) mission: design, execution, and first results, Atmos. Chem. Phys., 10, 5191–5212, doi:10.5194/acp-10-5191-2010, 2010. 29116, 29117, 29123
Kaufman, Y., Koren, I., Remer, L., Rosenfeld, D., and Rudich, Y.: The effect of smoke, dust, and pollution aerosol on shallow cloud development over the Atlantic Ocean, Proc. Natl. Acad. Sci., 102, doi:10.1073/pnas.0505191102, 2005. 29115, 29116, 29129
King, M. D., Platnick, S., Kaufman, D., Tanre, B. C., Menzel, W. P., Remer, L. A., Ackerman, S. A., and Gao, S.: Cloud and aerosol properties, precipitable water, and profiles of temperature and humidity from MODIS, IEEE Trans. Geosci. Remote Sens., 41, 442–458, 2003. 29121
King, M. D., Platnick, S. E., Hubanks, P. A., Arnold, T. G., and Wind, B.: Collection 005 Change Summary for the MODIS Cloud Optical Property Algorithm, NASA Tech Report, http://modis-atmos.gsfc.nasa.gov/products_C005update.html), 2005. 29120, 29143
Klein, S. A. and Hartmann, D. L.: The Seasonal Cycle of Low Stratiform Clouds., J. Climate, 6, 1587–1606, doi:10.1175/1520-0442(1993)006⟨1587:TSCOLS⟩2.0.CO;2, 1993. 29133
Law, K. S. and Stohl, A.: Arctic Air Pollution: Origins and Impacts, Science, 315, doi:10.1126/science.1137695, 2007. 29114, 29122, 29132
Lihavainen, H., Kerminen, V.-M., and Remer, L. A.: Aerosol-cloud interaction determined by both in situ and satellite data over a northern high-latitude site, Atmos. Chem. Phys. Discuss., 9, 27465–27483, doi:10.5194/acpd-9-27465-2009, 2009. 29129
Lohmann, U. and Feichter, J.: Global indirect aerosol effects: a review, Atmos. Chem. Phys., 5,

ACPD
10, 29113–29152, 2010

715–737, doi:10.5194/acp-5-715-2005, 2005. 29117, 29129
Longley, I., Inglis, D., Gallagher, M., Williams, P., and Allen, J.: Using NO_x and CO monitoring data to indicate fine aerosol number concentrations and emissions factors in three UK conurbations, Atmos. Environ., 39, 5157–5169, doi:10.1016/j.atmosenv.2005.05.017, 2005. 29117, 29127
Lu, M. L. and Seinfeld, J. H.: Study of the Aerosol Indirect Effect by Large-Eddy Simulation of Marine Stratocumulus, J. Atmos. Sci., 62, 3909–3932, doi:10.1175/JAS3584.1, 2005. 29115
Lubin, D. and Vogelmann, A. M.: A climatologically significant aerosol longwave indirect effect in the Arctic, Nature, 439, 453–456, doi:10.1038/nature04449, 2006. 29115, 29119, 29127
Mauritsen, T., Sedlar, J., Tjernström, M., Leck, C., Martin, M., Shupe, M., Sjogren, S., Sierau, B., Persson, P. O. G., Brooks, I. M., and Swietlicki, E.: Aerosols indirectly warm the Arctic, Atmos. Chem. Phys. Discuss., 10, 16775–16796, doi:10.5194/acpd-10-16775-2010, 2010. 29115, 29119, 29127
Morrison, H. and Pinto, J. O.: Mesoscale modeling of springtime Arctic mixed-phase stratiform clouds using a new two-moment bulk microphysics scheme, J. Atmos. Sci., 62, 3683–3704, doi:10.1175/JAS3564.1, 2005. 29119
Morrison, H., Pinto, O. J., Curry, J. A., and McFarquhar, G. M.: Sensitivity of modeled arctic mixed-phase stratocumulus to cloud condensation and ice nuclei over regionally varying surface conditions, J. Geophys. Res., 113, doi:10.1029/2007JD008729, 2008. 29119, 29131
Myhre, G., Stordal, F., Johnsrud, M., Kaufman, Y. J., Rosenfeld, D., Storelvmo, T., Kristjansson, J. E., Berntsen, T. K., Myhre, A., and Isaksen, I. S. A.: Aerosol-cloud interaction inferred from MODIS satellite data and global aerosol models, Atmos. Chem. Phys., 7, 3081–3101, doi:10.5194/acp-7-3081-2007, 2007. 29129
Nakajima, T., Higurashi, A., and Penner, J. E.: A possible correlation between satellite-derived cloud and aerosol microphysical parameters, Geophys. Res. Lett., 28, 1171–1174, doi:10.1029/2000GL012186, 2001. 29129
Olivier, J. G. and Berdowski, J. J. M.: Global emission sources and sinks, in: "The Climate System", edited by: Berdowski, J., Guicherit, R., and Heij, B. J., Tech. rep., A. A. Balkema Publishers Swets Zeitlinger Publishers, Lisse, The Netherlands, 2001. 29122
Paris, J., Ciais, P., Nédélec, P., Ramonet, M., Belan, B. D., Arshinov, M. Y., Golitsyn, G. S., Granberg, I., Stohl, A., Cayez, G., Athier, G., Boumard, F., and Cousin, J. M.: The YAK-AEROSIB transcontinental aircraft campaigns: new insights on the transport of CO_2, CO and O_3 across Siberia, Tellus B, 60, 551–568, doi:10.1111/j.1600-0889.2008.00369.x, 2008.

ACPD
10, 29113–29152, 2010

29117, 29128, 29133
Pincus, R. and Baker, M. B.: Effect of precipitation on the albedo susceptibility of clouds in the marine boundary layer, Nature, 372, 250–252, doi:10.1038/372250a0, 1994. 29131
Platnick, S., King, M. D., Ackerman, S. A., and Riedi, J.: The MODIS Cloud Products: Algorithms and Examples From Terra, IEEE, Trans. Geosci. Remote Sens., 41, 459–473, doi:10.1109/TGRS.2002.808301, 2003. 29120, 29121
Pradeep Kumar, P., Broekhuizen, K., and Abbatt, J. P. D.: Organic acids as cloud condensation nuclei: Laboratory studies of highly soluble and insoluble species, Atmos. Chem. Phys., 3, 509–520, doi:10.5194/acp-3-509-2003, 2003. 29133
Quaas, J., Boucher, O., and Breon, F.: Aerosol indirect effects in POLDER satellite data and the Laboratoire de Météorologie Dynamique-Zoom (LMDZ) general circulation model, J. Geophys. Res., 109, D08205, doi:10.1029/2003JD004317, 2004. 29116
Quinn, P. K., Shaw, G., Andrews, E., Dutton, E. G., Ruoho-Airola, T., and Gong, S. L.: Arctic haze: current trends and knowledge gaps, Tellus B., 59, 99–114, doi:10.1111/j.1600-0889.2006.00238.x, 2007. 29114
Quinn, P. K., Bates, T. S., Baum, E., Doubleday, N., Fiore, A. M., Flanner, M. G., Garrett, T. J., and Koch, D.: Short-lived pollutants in the Arctic: their climate impact and possible mitigation strategies, Atmos. Chem. Phys., 8, 1723–1735, doi:10.5194/acp-8-1723-2008, 2008. 29132
Radke, L. F., Coakley, J. A., and King, M. D.: Direct and Remote sensing of observations of the effects of ships on clouds, Science, 246, 1146, doi:10.1126/science.246.4934.1146, 1989. 29115
Reid, J. S., Koppmann, R., Eck, T. F., and Eleuterio, D. P.: A review of biomass burning emissions part II: intensive physical properties of biomass burning particles, Atmos. Chem. Phys., 5, 799–825, doi:10.5194/acp-5-799-2005, 2005. 29128
Riedi, J., Marchant, B., Platnick, S., Baum, B., Thieuleux, F., Oudard, C., Parol, F., Nicolas, J.-M., and Dubuisson, P.: Cloud thermodynamic phase inferred from merged POLDER and MODIS data, Atmos. Chem. Phys. Discuss., 7, 14103–14137, doi:10.5194/acpd-7-14103-2007, 2007. 29122, 29143
Rivera-Carpio, C. A., Corrigan, C. E., Novakov, T., Penner, J. E., Rogers, C. F., and Chow, J. C.: Derivation of contributions of sulfate and carbonaceous aerosols to cloud condensation nuclei from mass size distributions, J. Geophys. Res., 101, 19 483–19 494, doi:10.1029/95JD01077, 1996. 29128, 29133
Sekiguchi, M., Nakajima, T., Suzuki, K., Kawamoto, K., and Rosenfeld, D.: A study of the

ACPD
10, 29113–29152, 2010

direct and indirect effects of aerosols using global satellite data sets of aerosol and cloud parameters, J. Geophys. Res., 108, doi:10.1029/2002JD003359, 2003. 29116, 29129
Shaw, G. E.: The Arctic Haze Phenomenon., Bull. Amer. Meteorol. Soc., 76, 2403–2414, doi:10.1175/1520-0477(1995)076⟨2403:TAHP⟩2.0.CO;2, 1995. 29116
Shupe, M. D., Matrosov, S. Y., and Uttal, T.: Arctic Mixed-Phase Cloud Properties Derived from Surface-Based Sensors at SHEBA, J. Atmos. Sci., 63, 697–711, doi:10.1175/JAS3659.1, 2006. 29121, 29124, 29126, 29131
Sirois, A. and Barrie, L. A.: Arctic lower troposphere aerosol trends and composition at Alert, Canada: 1980–1995, J. Geophys. Res., 104, 11599–11618, 1999. 29132
Stevens, B. and Feingold, G.: Untangling aerosol effects on clouds and precipitation in a buffered system, Nature, 461, 607–613, doi:10.1038/nature08281, 2009. 29131
Stohl, A.: POLARCAT White Paper, Tech. rep., NILU, http://www.polarcat.no/motivation, 2005. 29116
Stohl, A.: Characteristics of atmospheric transport into the Arctic troposphere, J. Geophys. Res., 111, D11 306, 2006. 29122, 29127, 29128, 29130
Stohl, A. and Thomson, D. J.: A Density Correction for Lagrangian Particle Dispersion Models, Bound.-Lay. Meteorol., 90, 155–167, doi:10.1023/A:1001741110696, 1999. 29122
Stohl, A., Forster, C., Frank, A., and Seibert, P.: Technical note: The Lagrangian particle dispersion model FLEXPART version 6.2, Tech. rep., NILU, 2005. 29122, 29143
Stohl, A., Andrews, E., Burkhart, J. F., Forster, C., Herber, A., Hoch, S. W., Kowal, D., Lunder, C., Mefford, T., Ogren, J. A., Sharma, S., Spichtinger, N., Stebel, K., Stone, R., Ström, J., Tørseth, K., Wehrli, C., and Yttri, K. E.: Pan-Arctic enhancements of light absorbing aerosol concentrations due to North American boreal forest fires during summer 2004, J. Geophys. Res., 111, D22214, doi:10.1029/2006JD007216, 2006. 29116
Stohl, A., Berg, T., Burkhart, J. F., Fjæraa, A. M., Forster, C., Herber, A., Hov, Ø., Lunder, C., McMillan, W. W., Oltmans, S., Shiobara, M., Simpson, D., Solberg, S., Stebel, K., Ström, J., Tørseth, K., Treffeisen, R., Virkkunen, K., and Yttri, K. E.: Arctic smoke – record high air pollution levels in the European Arctic due to agricultural fires in Eastern Europe in spring 2006, Atmos. Chem. Phys., 7, 511–534, doi:10.5194/acp-7-511-2007, 2007. 29116, 29122, 29143
Twomey, S.: The Influence of Pollution on the Shortwave Albedo of Clouds, J. Atmos. Sci., 34, 1149–1154, doi:10.1175/1520-0469(1977)034⟨1149:TIOPOT⟩2.0.CO;2, 1977. 29115
Vestin, A., Rissler, J., Swietlicki, E., Frank, G. P., and Andreae, M. O.: Cloud-nucleating

ACPD
10, 29113–29152, 2010

properties of the Amazonian biomass burning aerosol: Cloud condensation nuclei measurements and modeling, J. Geophys. Res., 112, D14201, doi:10.1029/2006JD008104, 2007. 29128, 29133

Warneke, C., Bahreini, R., Brioude, J., Brock, C. A., de Gouw, J. A., Fahey, D. W., Froyd, K. D., Holloway, J. S., Middlebrook, A., Miller, L., Montzka, S., Murphy, D., Peischl, J., Ryerson, T. B., Schwarz, J., Spackman, J. R., and Veres, P.: Biomass burning in Siberia and Kazakhstan as an important source for haze over the Alaskan Arctic in April 2008, Geophys. Res. Lett., 36, doi:10.1029/2008GL036194, 2009. 29133

Warneke, C., Froyd, K. D., Briode, J., and Stohl, A.: An important contribution to springtime Arctic aerosol from biomass burning in Russia, Geophys. Res. Lett., 37, L01801, doi:10.1029/2009GL041816, 2010. 29123, 29133

Weisz, E., Li, J., Menzel, W. P., Heidinger, A. K., and Kahn, B. H.: Comparison of AIRS, MODIS, CloudSat and CALIPSO cloud top height retrievals, Geophys. Res. Lett., 34, L17811, doi:10.1029/2007GL030676, 2007. 29121

White, P. W.: IFS Documentation, http://www.ecmwf.int, Tech. rep., ECMWF, Reading, UK, 2002. 29122

Wood, R.: Cancellation of aerosol indirect effects in marine stratocumulus through cloud thinning, J. Atmos. Sci., 64, 2657–2669, doi:10.1175/JAS3942.1, 2007. 29131

Xue, H. and Feingold, G.: Large eddy simulations of trade wind cumuli: Investigation of aerosol indirect effects, J. Atmos. Sci., 1605–1622, doi:10.1175/JAS3706.1, 2006. 29115

Table 1. Cloud products and pollution tracer used in the study.

Source	Parameter	Reference
MODIS - Aqua	Cloud top temperature (T_C)	
	Cloud optical depth (τ)	
	Droplet effective radius (r_e)	(King et al., 2005)
POLDER -PARASOL	Cloud pressure (P_{O_2})	(Fougnie et al., 2007)
MODIS-POLDER	Cloud phase index (ϕ)	(Riedi et al., 2007)
FLEXPART	Anthropogenic & biomass burning tracer (χ_{CO})	(Stohl et al., 2005, 2007)

ACPD
10, 29113–29152, 2010

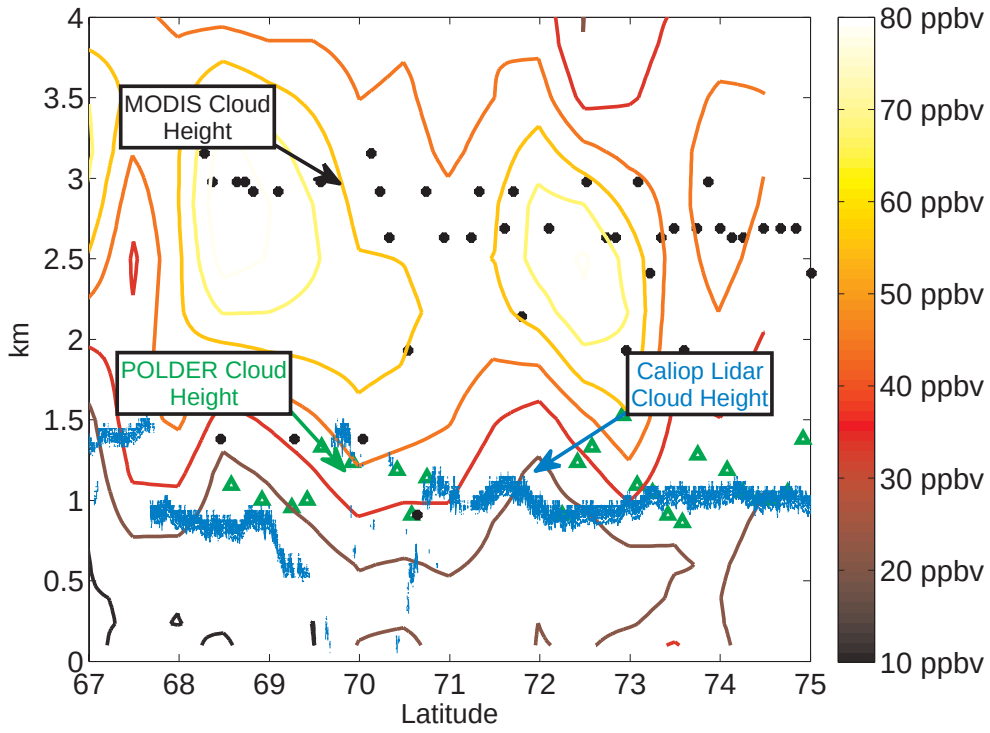

Fig. 1. Cloud top heights from the A-train instruments MODIS (black dots), POLDER (green Δ) and CALIOP (blue dash), corresponding to a visually identified stratiform cloud deck in the White Sea, plotted with FLEXPART pollution tracer output (Contours) modeling anthropogenic and biomass burning CO emissions.

ACPD
10, 29113–29152, 2010

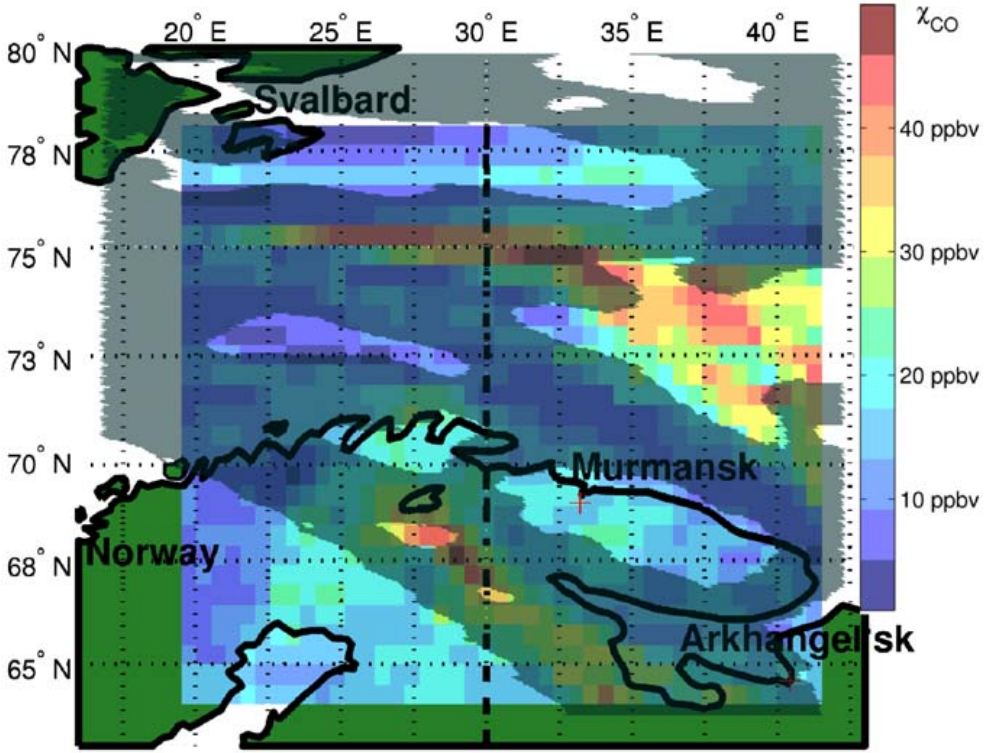

Fig. 2. Illustration of the horizontal and vertical co-location method, showing cloud with pressures from POLDER between 800 hPa and 900 hPa (gray shading) and average χ_{CO} concentrations in ppbv for a layer between 1 km to 2 km altitude, colored shading. The dotted line is the location of the vertical transect shown in Fig. 3.

ACPD
10, 29113–29152, 2010

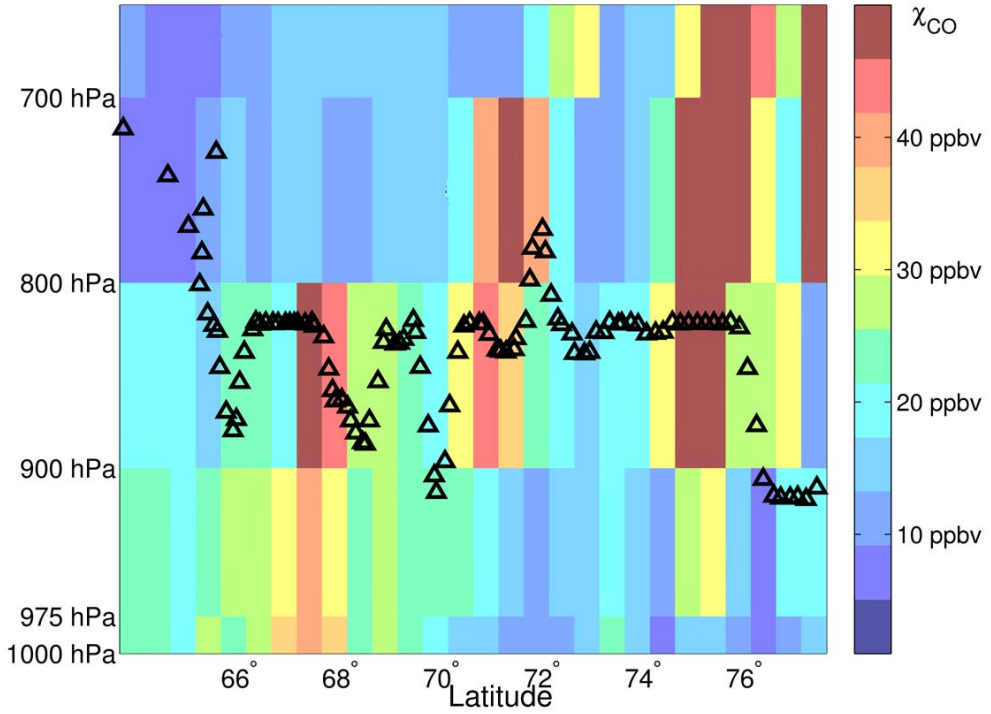

Fig. 3. Illustration of the vertical co-location method used for satellite cloud data and chemical tracer transport model output. The colors represent values of the CO pollution tracer for a vertical slice along the 30° East meridian shown in Fig. 2. The Δ represent the POLDER retrieved cloud top pressure. After co-locating fields of cloud properties both horizontally and temporally, the cloud top pressure is matched to the output of the FLEXPART model that corresponds to the vertical location of the cloud.

ACPD
10, 29113–29152, 2010

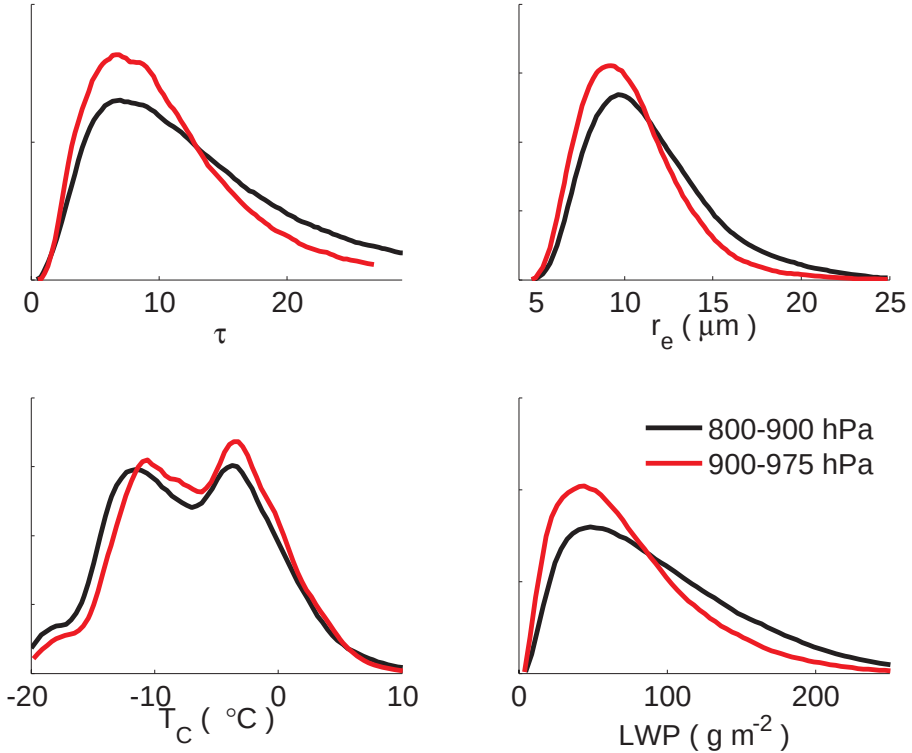

Fig. 4. Probability distribution functions for cloud optical depth (τ), effective radius (r_e), cloud top temperature (T_C) and liquid water path (LWP) for liquid, low-level Arctic clouds north of 65°N, sampled over the period 20 March and 20 July 2008. For the vertical layers 800 hPa to 900 hPa and 900 hPa to 975 hPa, respectively, there were 282 953 and 146 373 0.5° × 0.5° FLEXPART grid cells containing at least 50% cloud cover.

ACPD
10, 29113–29152, 2010

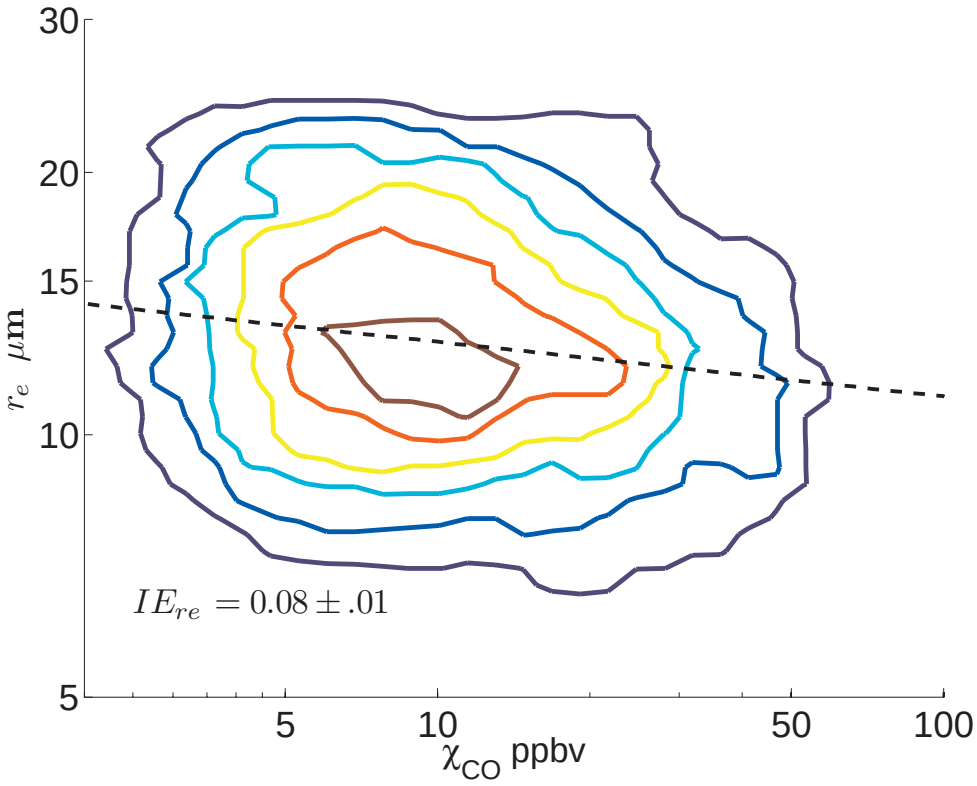

Fig. 5. Calculation of the IE parameter from a distribution of values of r_e and χ_{CO} for liquid clouds in the Arctic with cloud top pressures between 800 and 900 hPa and cloud top temperatures between 0 °C and 2 °C. Color scale indicates a higher density of values.

ACPD
10, 29113–29152, 2010

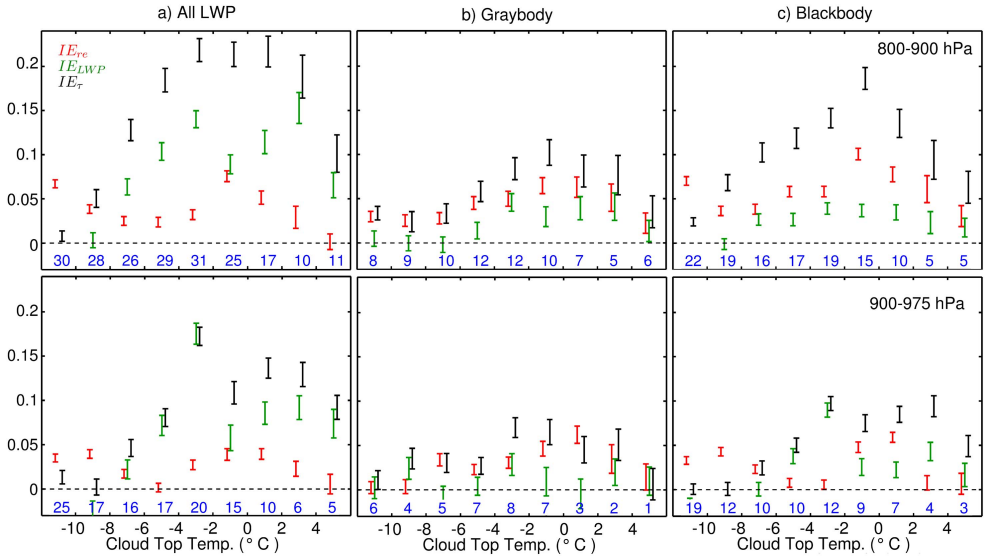

Fig. 6. IE parameter as a function of temperature calculated for liquid clouds ($\phi < 50$) north of 65° N from 20 March through 20 July 2008 for the layers 800–900 hPa (Row 1) and 900–975 hPa (Row 2). The bars indicate the 95% confidence limit in the calculation of IE. The figures are grouped according to; **(a)** all LWP, **(b)** graybody clouds with LWP < 40 g m^{-2} or **(c)** blackbody clouds with LWP > 40 g m^{-2}. Blue numbers indicate how many FLEXPART grid boxes containing clouds, in thousands, went into the calculation of the IE parameter.

ACPD
10, 29113–29152, 2010

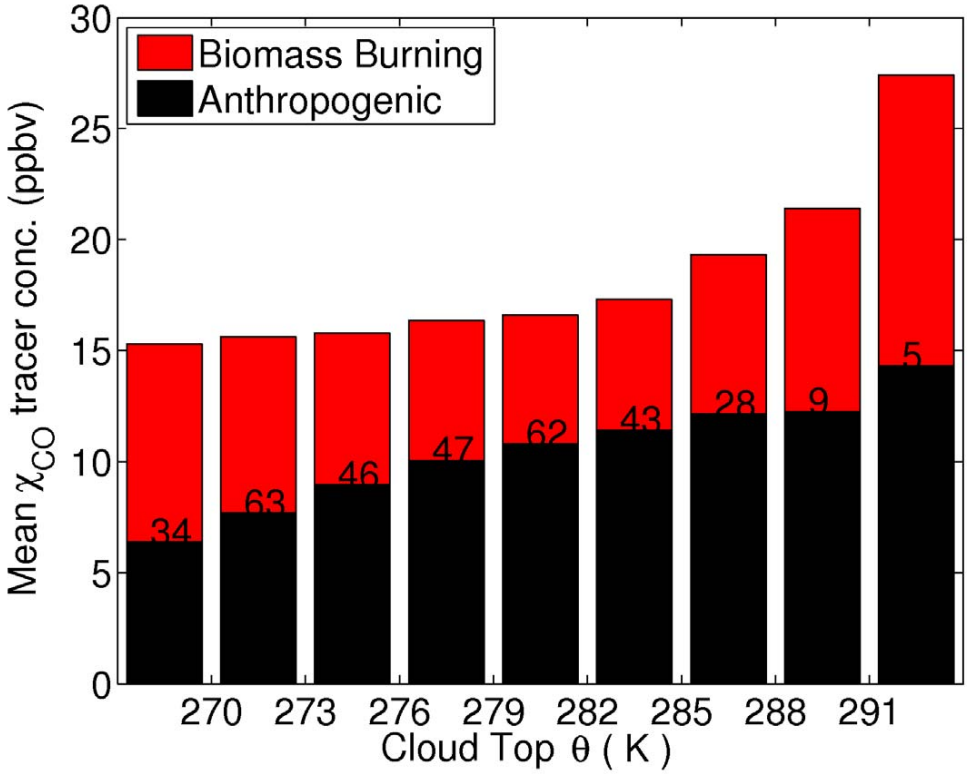

Fig. 7. Mean χ_{CO} concentrations from anthropogenic and biomass burning sources, for clouds below 800 hPa, binned by cloud top potential temperatures shown on the bottom axis. Numbers, in thousands, indicate how many FLEXPART grid boxes with liquid clouds, at that potential temperature, were averaged together.

ACPD
10, 29113–29152, 2010

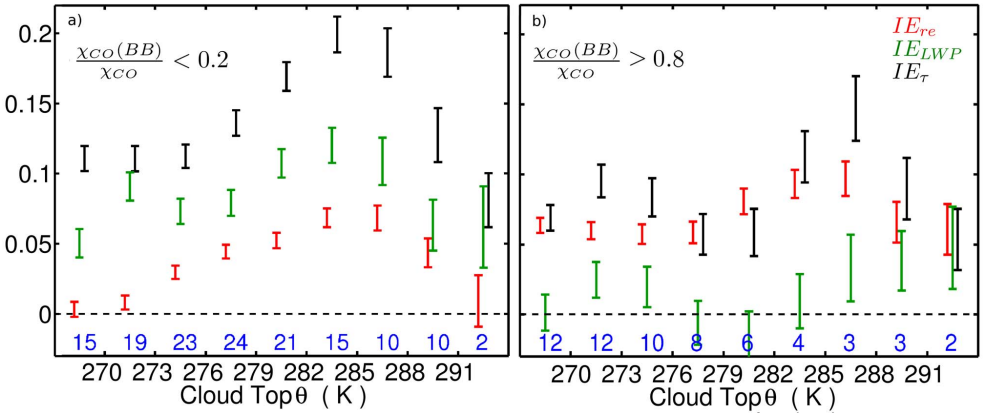

Fig. 8. As for Fig. 5 except the plots represent IE values plotted within 3 K bins in potential temperature for Arctic clouds coincident with biomass burning χ_{CO} concentrations that are either **(a)** >80% or **(b)** <20% of the total χ_{CO} concentrations.

ACPD
10, 29113–29152, 2010

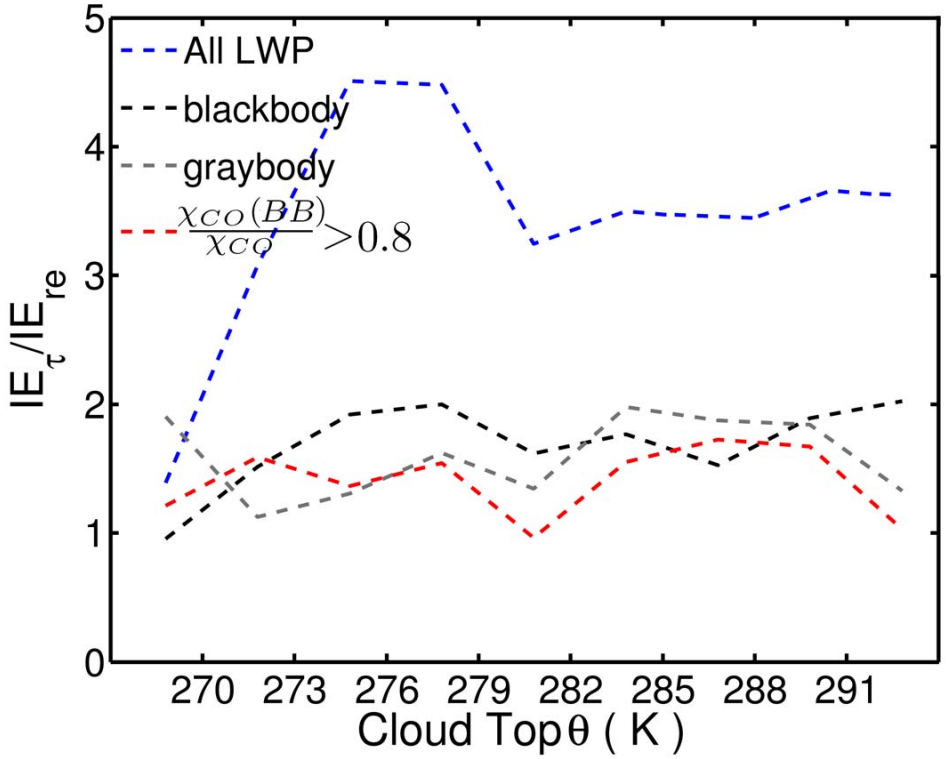

Fig. 9. Enhancement of IE_τ over IE_{r_e} as a function of potential temperature and LWP, for low-level liquid clouds in the Arctic from 20 March to 20 July 2008. The enhancements are plotted according to; (blue) all LWP, (gray) graybody clouds with LWP <40 gm^{-2} , (black) blackbody clouds with LWP > 40 gm^{-2} or (red) with biomass burning (BB) χ_{CO} > 0.8 of the total χ_{CO} concentrations.

ACPD
10, 29113–29152, 2010